Effect of homogenization treatment and micro-alloying with Mn on the microstructure and hot workability of AA6060 aluminum alloys

Xiaoming Qian [1], Nick Parson [2], X. Grant. Chen [1, *]

[1] Department of applied sciences, University of Quebec at Chicoutimi, Saguenay, QC, Canada, G7H 2B1
*(*Corresponding author: xgrant_chen@uqac.ca (X. Grant Chen))*

[2] Arvida Research and Development Centre, Rio Tinto, Saguenay QC, Canada, G7S 4K8

Abstract

The effects of a homogenization treatment and micro-alloying with Mn on the evolution of the microstructure and hot workability of AA6060 aluminum alloys were investigated. Various homogenization treatments with temperatures ranging from 520 to 610 °C and soaking times from 2 to 16 h were conducted. The results revealed that β-AlFeSi intermetallic was the dominant phase in the as-cast microstructure of the experimental alloys. During the homogenization, the fragmentation of intermetallics occurred and plate-like β-AlFeSi transformed into rod-like α-AlFeSi. In addition, a number of dispersoids precipitated in the 0.1Mn alloy in the temperature range of 520 to 580 °C. The flow stress behavior of the homogenized AA6060 alloys was mainly determined by the solid solution level. Increasing homogenization temperatures resulted in higher flow stresses owing to the increase in solute atoms in the aluminum matrix. The incremental Mn addition from 0 to 0.1% moderately increased the flow stress by up to 3%. Grain growth occurred in the alloys with low Mn contents (<0.03Mn) during the high-temperature homogenization (580–610 °C), which resulted in a sudden decrease in the flow stresses and an irregular sample shape after the deformation. Micro-alloying with Mn (>0.06%) can effectively prevent grain growth at such temperatures. For an alloy with Mn (0.1%) micro-alloying, homogenization at 550–580 °C for 6 h could be the optimal condition to balance the flow stress and desirable microstructure.

Keywords: AA6060 alloys, Homogenization, Micro-alloying of Mn, Hot deformation, Flow stress

1 Introduction

Over the last decades, the consumption and demand for aluminum alloys have rapidly grown owing to their light weight, high strength-to-weight ratio, and easy recyclability. AA6060 aluminum alloys are typically used for extrusion parts with complex cross sections in automobile and architectural applications because they possess a combination of medium strength, excellent formability, good corrosion resistance and anodizing properties. AA6060 extrusion billets are mostly produced via direct chill (DC) casting, during which the non-equilibrium solidification induces an inhomogeneous microstructure such as micro-segregations and a network of brittle Fe-bearing intermetallics, thereby causing a low formability (Ref. 1, 2). In general, the homogenization is conducted before the extrusion to eliminate such negative effects. During a homogenization, the micro-segregation of the alloying elements at dendrite boundaries can be diminished, and a more uniform element distribution can be achieved (Ref. 3). On the other hand, the interdendritic network of plate-like β-AlFeSi intermetallics is gradually replaced by more rounded and discrete α-AlFeSi intermetallic particles (Ref. 4–6). The precipitation of secondary particles (dispersoids) can occur in Mn- and Cr-containing alloys (Ref. 7, 8). A proper homogenization regime can significantly increase the extrusion productivity and benefit the surface finish (Ref. 9, 10).

It is well known that the addition of Mn to 6xxx aluminum alloys can modify the microstructure of as-cast and heat-treated samples and thus improve the alloy properties (Ref. 11–13). In AA6xxx alloys, Mn is present in constituent particles, fine dispersoids, and solid solutions. Kuijpers et al. (Ref. 14) reported that during the homogenization of Al–Mg–Si alloys, β-AlFeSi transformed into α-Al(FeMn)Si intermetallics. Lodgaard and Ryum (Ref. 8) reported that Mn-bearing dispersoids started to form at 400 °C during the homogenization of Al–Mg–Si alloys. Shakiba et al. (Ref. 15) reported that Mn addition to dilute Al–Fe–Si alloys increased the high-temperature flow stress owing to the increased Mn solid solution level.

Several research works have been performed to investigate the impact of the homogenization treatment on the microstructure evolution and Fe-rich intermetallic transformation in Al-Mg-Si 6xxx alloys (Ref. 16-20). Bryantsev (Ref. 16) performed a quantitative analysis of the transformation of Fe-containing intermetallics during homogenization as a function of temperature and soaking time in 6xxx alloys. Haidemenopoulos et al. (Ref. 17) carried out a computational simulation of the β-AlFeSi to α-AlFeSi transformation via integrating the process steps from solidification to

homogenization. Recently, Liu et al. (Ref. 18) built a predictive model for the evolution of critical microstructural features on spatial distribution of solutes, constituent particles and dispersoids during homogenization of AA6082 alloy based on the experiment results. However, most of the researches focused on the microstructure changes during homogenization, but the corresponding effect on the downstream properties such as hot workability was rarely addressed. In addition, AA6060 alloys contain a relatively low alloying element content (0.3-0.6Mg, 0.3-0.6Si) among 6xxx alloys, which makes them relatively soft after homogenization and can be extruded at a high speed. Therefore, even a small reduction in the flow stress can greatly increase the extrusion speed and improve the productivity. However, the effect of micro-alloying of Mn on the microstructure change during homogenization and its influence on the hot workability are still far being clear.

In the present study, the effects of the homogenization and micro-alloying with Mn on the evolution of the microstructure and hot workability of AA6060 were investigated systematically. The as-cast and homogenized microstructures were examined, and the true stress–strain response was obtained by conducting hot-compression tests. The focus of this study is the relation between the microstructure, solid solution levels, and hot workability.

2 Experiments

Four AA6060 alloy samples with micro-alloying additions of 0–0.1 wt.% Mn were used. The chemical compositions are shown in Table 1. All alloy compositions are in wt.% unless otherwise indicated. The sample materials were taken from DC cast billets with a diameter of 101 mm, provided by the Arvida Research and Development Center of Rio Tinto based in Saguenay, Quebec. The billets were homogenized at 520, 550, 580, and 610 °C for 2, 6, and 16 h and finally water-quenched. Afterward, the samples were prepared with standard metallographic procedure for the microstructure observation. To reveal more details of the microstructure, some of the polished samples were etched with a 0.5% HF solution for 40 s. An optical microscope (Nikon, Eclipse ME600), a scanning electron microscope (SEM, JEOL-6480LV), and transmission electron microscope (TEM, JEM−2100) were used to examine the microstructures. Moreover, a quantitative analysis of the dispersoid particle distributions was performed based on the SEM images of the etched surfaces. The electrical conductivity was measured with a Sigmascope SMP10 eddy-current device at room temperature to estimate the solid solution levels. Six measurements were performed for each sample to provide an average value. Further,

cylindrical specimens of 10 mm diameter and 15 mm height were machined for the hot-compression tests. The uniaxial hot-compression tests were performed using a Gleeble 3800 thermo-mechanical testing unit. The specimens were heated at 2 °C/s and held to 500° C for 180 s to ensure a homogeneous temperature distribution. Next, the specimens were deformed to a total true strain of 0.8 at a strain rate of 1 s^{-1}.

Table 1 Chemical composition of investigated alloys (wt.%)

Alloys	Mg	Si	Fe	Mn	Al
Base alloy	0.37	0.50	0.17	-	Bal.
0.03Mn	0.37	0.50	0.17	**0.03**	Bal.
0.06Mn	0.37	0.50	0.17	**0.06**	Bal.
0.1Mn	0.37	0.51	0.19	**0.09**	Bal.

3 Results and discussion

3.1 As-cast microstructure

The as-cast microstructure of the base alloy is shown in Fig. 1. As indicated in Fig. 1a, it was composed of aluminum dendrite cells, β-AlFeSi intermetallic distributed along the dendrite boundaries, a small amount of α-AlFeSi intermetallic located within the dendrite cells, and primary Mg_2Si particles. Figs. 1b and 1c show enlarged SEM images of the β-AlFeSi and α-AlFeSi intermetallics, which exhibited plate-like and blocky morphologies, respectively. Figs. 1c and 1d illustrate that the small primary Mg_2Si particles were mostly co-located with α- and β-AlFeSi intermetallics. In the as-cast microstructure, β-AlFeSi intermetallic was the predominant phase, whereas α-AlFeSi and Mg_2Si were the minor phases. Regarding the three Mn-containing alloys, the as-cast microstructures were similar to that of the base alloy, thereby indicating that the presence of minor Mn had approximately no effect on the as-cast microstructure. Therefore, only the typical microstructure of the base alloy is presented here.

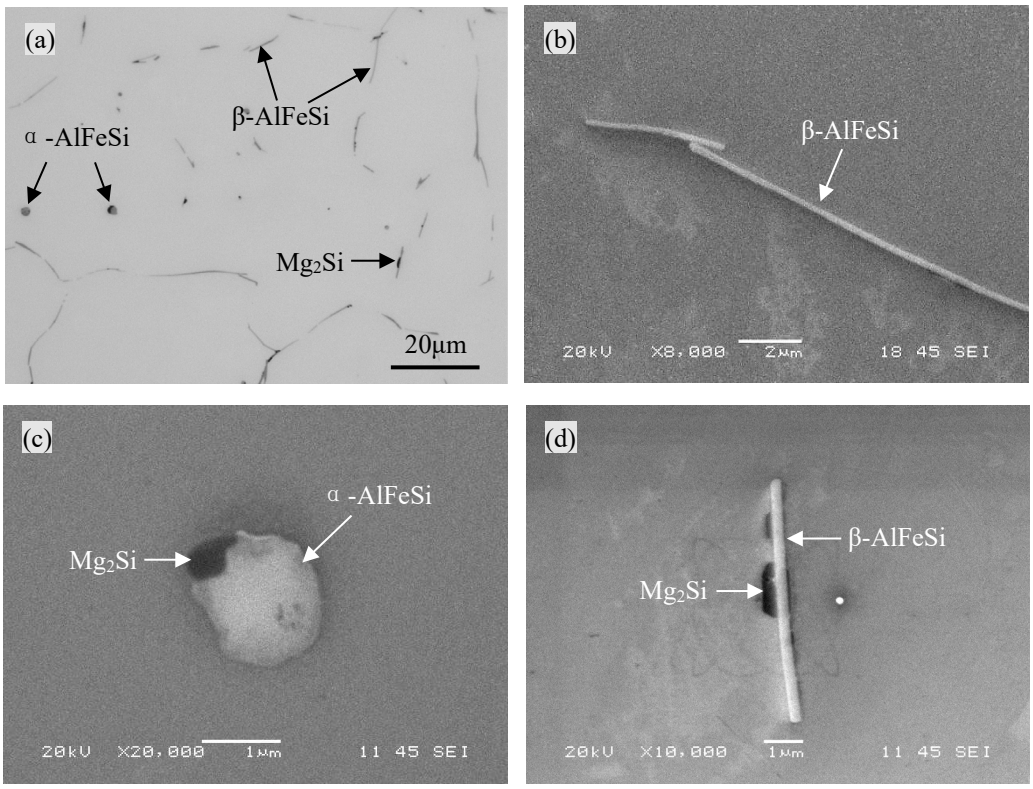

Fig. 1 As-cast microstructure of the base alloy, (a) optical image and (b) – (d) backscatter SEM images: (b) β-AlFeSi intermetallic, (c) α-AlFeSi intermetallic with co-located primary Mg_2Si particle and (d) Mg_2Si particles co-located with β-AlFeSi.

3.2 Microstructure after homogenization

The homogenized microstructures of the base and 0.1Mn alloys are shown in Figs. 2 and 3 for 520, 550, 580, and 610 °C and soaking times of 2, 6, and 16 h. In general, a fragmentation of β-AlFeSi intermetallics was observed in both alloys. Large plate-like β-AlFeSi particles were gradually replaced by separate particles. Increasing homogenization temperatures and longer soaking times promoted the fragmentation process. In addition, dispersoids precipitated in the 0.1Mn alloy at 520–580 °C and were visible after the HF etching (Fig. 3).

During the homogenization, the phase transformation from plate-like β-AlFeSi to more rounded and discrete α-AlFeSi occurred in both base and 0.1Mn alloys. Both phases were confirmed via the SEM–EDX analyses. Regarding the homogenized base alloy at 550 °C and below, the Fe-bearing intermetallic remained in the form of β-AlFeSi. During the homogenization at 580 °C, β-AlFeSi began to transform into α-AlFeSi. By contrast, in the 0.1Mn alloy, the transformation of β-AlFeSi into α-Al(FeMn)Si already

started at 520 °C. The promotion of the transformation of β-AlFeSi into α-Al(FeMn)Si at lower temperatures by the addition of Mn is in line with the results from previous studies (Ref. 19). Fig. 4 shows typical α-AlFeSi/α-Al(FeMn)Si particles in the base and 0.1Mn alloys after a homogenization at 580 °C for 6 h. They exhibit a rod-like morphology with rounded edges.

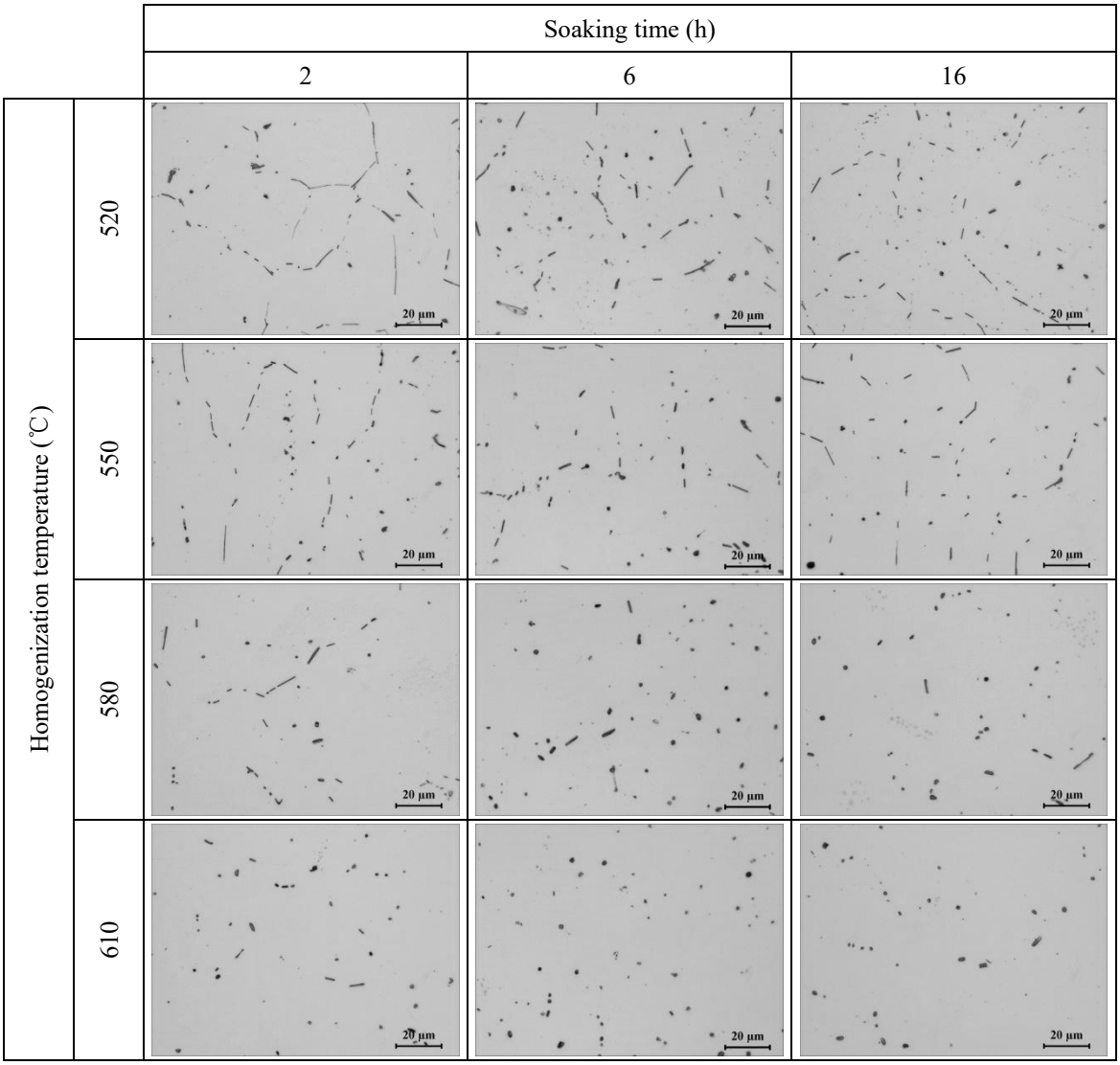

Fig. 2 Optical microstructure after homogenization of the base alloy under different conditions (0.5% HF/40 s etched)

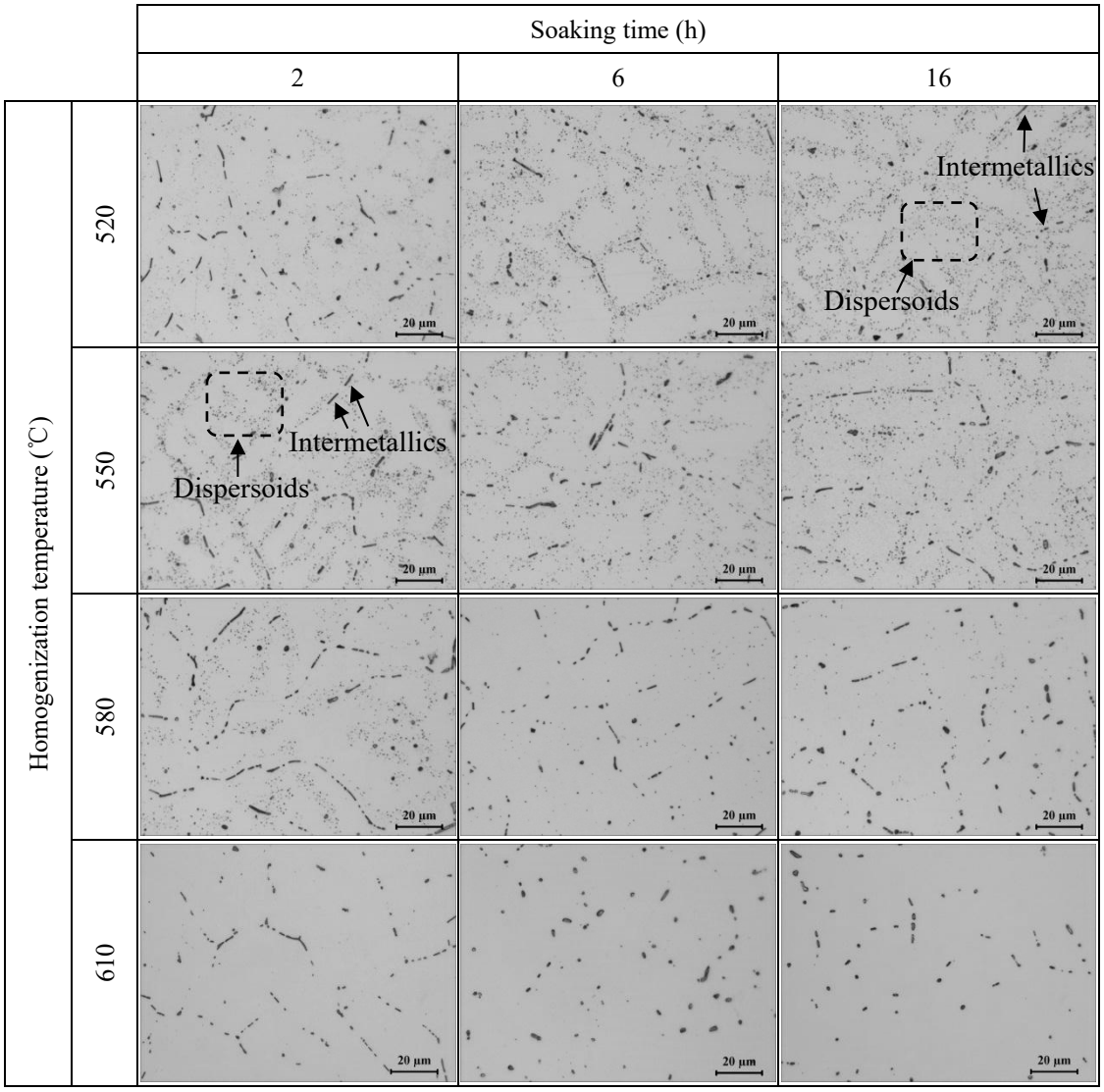

Fig. 3 Optical microstructure after homogenization of the 0.1Mn alloy under different conditions (0.5% HF/40 s etched)

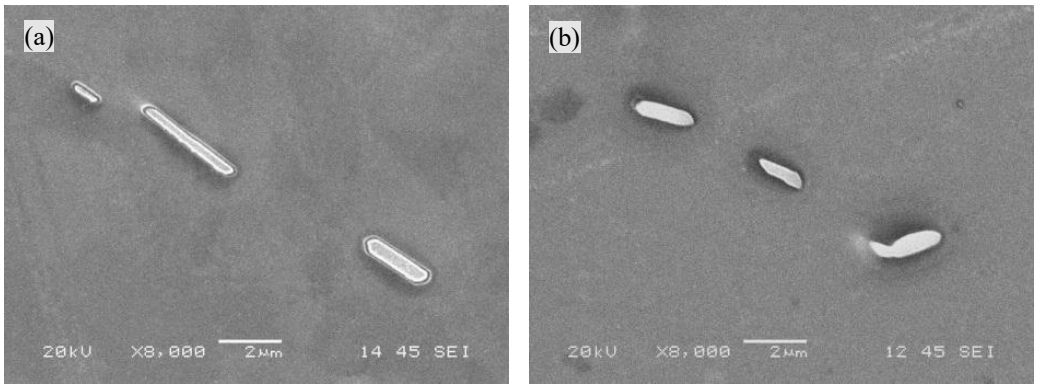

Fig. 4 SEM images (a) α-AlFeSi in the base alloy and (b) α-Al(FeMn)Si in the 0.1Mn alloy after homogenization at 580°C for 6 h

The blocky α-AlFeSi intermetallics that pre-existed in the as-cast microstructure (Fig. 1c) were not modified by the homogenization, whereas all primary Mg_2Si particles (Figs. 1c and d) were dissolved. Enlarged typical dispersoids are presented in Fig. 5 for the 0.1Mn alloy after a homogenization at 520 °C for 6 h. According to the TEM–EDX analysis, the dispersoids were confirmed to be the an α-Al(FeMn)Si phase (Figs. 5b and c), which agrees well with the results in (Ref. 20).

Fig. 6 shows the evolution of the number density and average equivalent diameter of the dispersoid particles after homogenizations under different conditions, measured via an image analysis of a series of SEM images of etched surfaces, an example of which is shown in Fig. 5a. During the homogenization at 520 °C, the dispersoid number density increased with increasing soaking time from $0.10/\mu m^2$ after 2 h to $0.24/\mu m^2$ after 16 h. The equivalent diameter increased from 0.50 μm after 2 h to 0.82 μm after 16 h. At 550 °C, the dispersoid number density started to decrease with increasing soaking time. The equivalent diameter initially decreased slightly from 0.62 μm (2 h) to 0.52 μm (6 h) and then increased to 0.75 μm after 16 h, indicating a coarsening process at this temperature. At 580 °C, only dispersoids with low number densities were observed after 2 h soaking. They nearly disappeared with increasing time, which indicates their dissolution. With a further increase in temperature to 610 °C, no dispersoids were observed in the aluminum matrix.

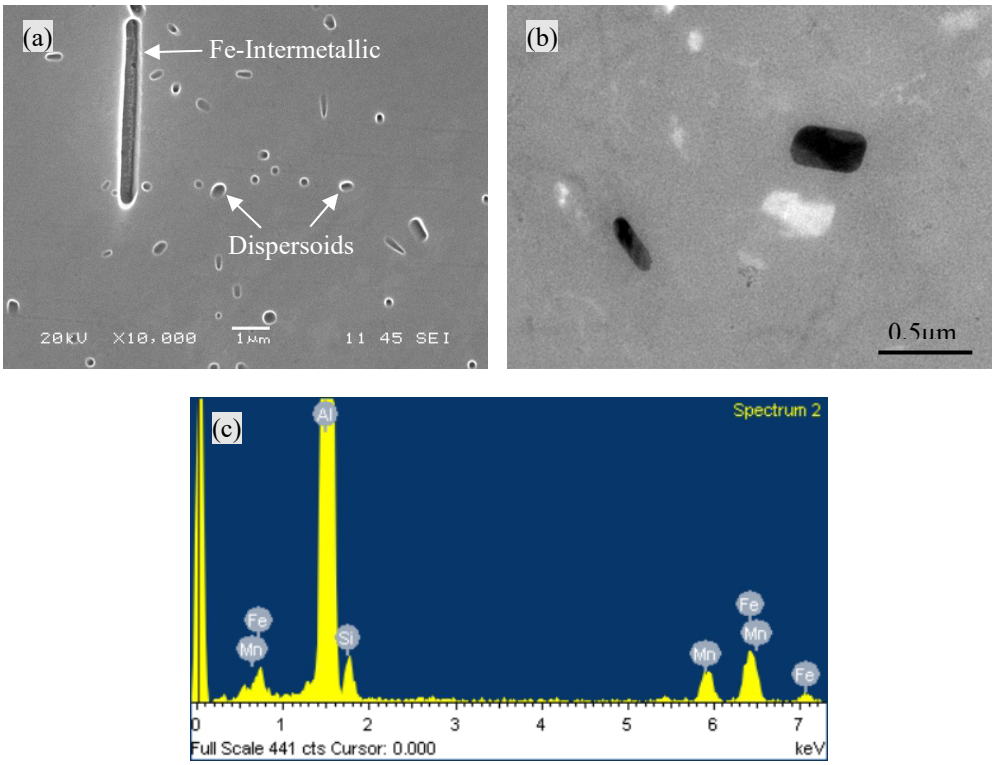

Fig. 5 Dispersoids in the 0.1Mn alloys homogenized at 520°C for 6 h: (a) SEM image, (b) TEM bright field image and (c) TEM-EDX spectra image.

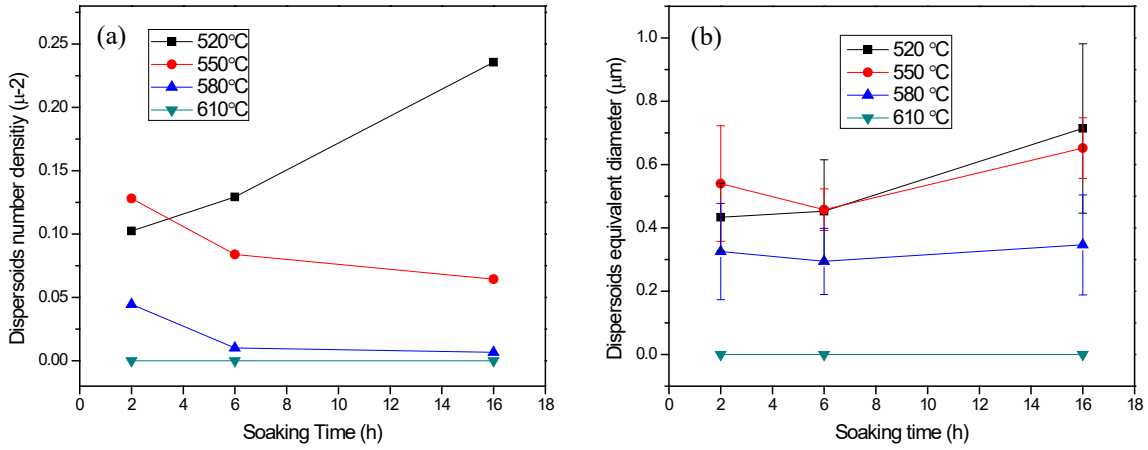

Fig. 6 Evolution of the number density (a) and average equivalent diameter (b) of dispersoids during homogenization for the 0.1Mn alloy

3.3 Solid solution levels

Solid solution levels can have a significant effect on the mechanical properties and high-temperature flow stress in aluminum alloys (Ref. 21–23). The change in the electrical conductivity was used as an indicator to investigate the solid solution level change during the homogenization. The effects of the homogenization treatment on the electrical conductivity are shown in Fig. 7. Regarding the Mn-free base alloy (Fig. 7a), the as-cast sample exhibited the highest electrical conductivity, which corresponds to the lowest solid solution level. This can be attributed to a portion of the main alloying elements (Mg, Si, and Fe) in the primary Mg_2Si and Fe-bearing intermetallics (Fig. 1). After the homogenization, the electrical conductivity decreased with increasing homogenization temperature. For example, for a fixed soaking time of 6 h, the electrical conductivity of the base alloy decreased from 50.89 to 50.7, 50.39, and 49.92 IACS as the temperature increased from 520 to 550, 580, and 610 °C, respectively. In addition, the electrical conductivity remained approximately constant with increasing soaking time. The decrease in the electrical conductivity reflects the increase in the solid solution levels at higher homogenization temperatures, which corresponds to more solute being released from the alloying elements (Mg, Si, and Fe) into the aluminum matrix owing to the dissolution of primary Mg_2Si and the fragmentation of Fe-bearing intermetallics.

Compared with the base alloy, the 0.1Mn alloy exhibited a significantly lower electrical conductivity, which corresponds to higher solid solution levels after the Mn addition. With a similar tendency as the base alloy, the electrical conductivity of the 0.1Mn alloy decreased with increasing homogenization temperature owing to the increased solid solubility limits. In contrast to that of the base alloy, the conductivity increased for longer soaking times. This indicates that the Mn level in the matrix decreased for longer soaking times.

Fig. 8 presents the Mn/Fe ratio of intermetallics in the 0.1Mn alloy for all experimental conditions measured via SEM–EDX. In as-cast condition, only β-AlFeSi intermetallic presented in the 0.1 Mn-containing alloy (Fig. 1). The Mn/Fe ratio of intermetallics was close to 0, because β-AlFeSi intermetallic was free of Mn. During transformation of β-AlFeSi to α-AlFeSi in the homogenization process, the Mn/Fe ratio increased with higher homogenization temperature and longer soaking time, thereby indicating the loss of Mn solute from the aluminum matrix with prolonged soaking time. The Mn atoms diffused from the aluminum matrix into Fe-bearing intermetallic during the transformation. It suggests that the trends in Fig. 8 are due to a continued long-range diffusion of Mn into the constituent particles with increasing time and temperature. Replacement of some Fe atoms by Mn in Fe-bearing intermetallics was reported in (Ref. 19), when the transformation of β-AlFeSi to α-AlFeSi in aluminum alloys occurred. Similar effects were reported for AA6082 alloys with higher Mn contents (Ref. 20, 24).

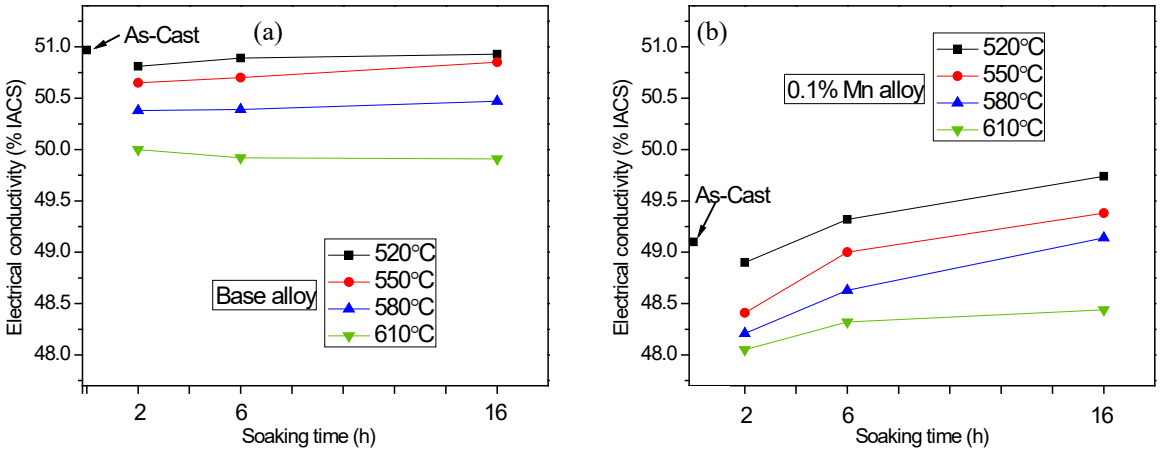

Fig. 7 Electrical conductivity of (a) the base alloy and (b) 0.1Mn alloy after different homogenization conditions

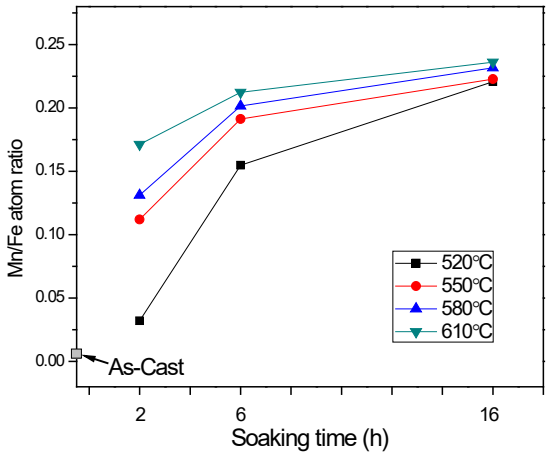

Fig. 8 Mn/Fe ratio of intermetallics in the 0.1Mn alloy for different homogenization conditions

3.4 Flow stress behavior during hot deformation

The hot workability was assessed via compression tests performed at 500 °C and a strain rate of 1 s^{-1}. The test temperature was deliberately selected to be above the Mg_2Si solvus temperature (~ 472 °C for those alloys) to avoid any interactions with Mg_2Si precipitation/dissolution effects. Figs. 9 and 10 show the true stress–strain curves of the base and 0.1Mn alloys for the respective homogenization conditions. In most cases, the flow stress increased rapidly at the beginning of the deformation. Shortly afterward, the

flow stress experienced a slow increase until the end of the deformation process, indicating that the dynamic work hardening was slightly stronger than the dynamic softening. In all compression tests for both alloys, the flow stress levels varied within a relatively narrow range of 27–32 MPa for a strain of 0.75. However, this represents a difference of approximately 15%, which is significant in terms of commercial extrusion productivity.

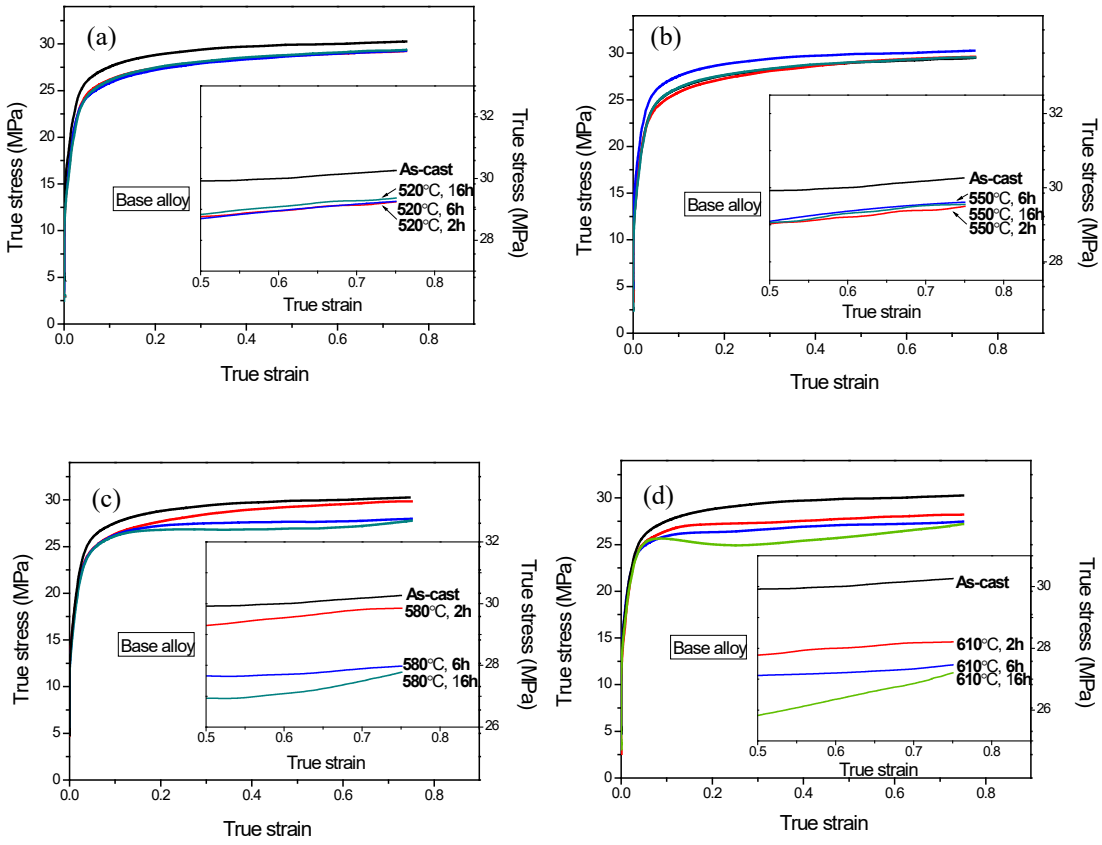

Fig. 9 True stress-strain curves of the base alloy at different homogenization conditions, (a) 520 °C, (b) 550 °C, (c) 580 °C and (d) 610 °C

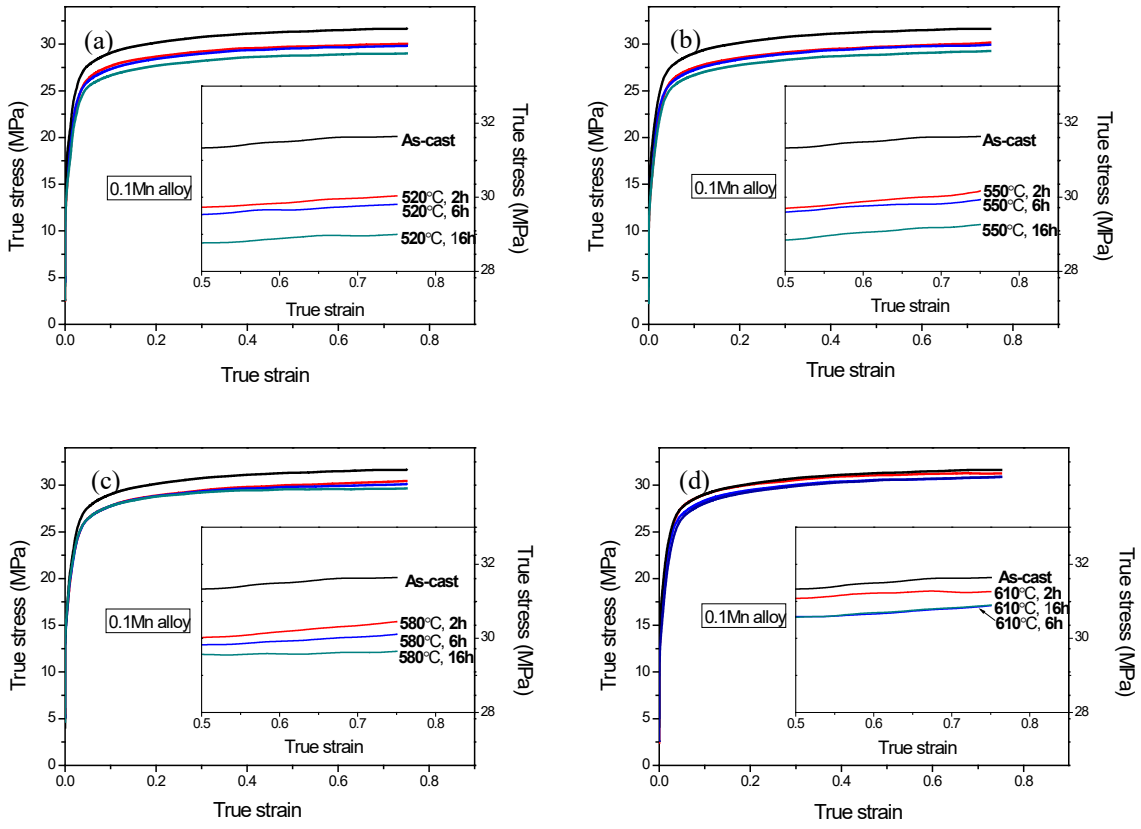

Fig. 10 True stress-strain curves of the 0.1Mn alloy at different homogenization conditions, (a) 520 °C, (b) 550 °C, 9c) 580 °C and (d) 610 °C

To better compare the effect of the homogenization on the hot workability, the flow stress values at a strain of 0.75 are plotted in Fig. 11 as a function of soaking temperature and time. In both alloys, the as-cast sample always exhibited the highest flow stress compared with the samples that experienced homogenization. This is probably due to the inter-connected network of Fe-bearing intermetallics surrounding the aluminum dendrite cell/grain boundaries (Fig. 1a). Regarding the base alloy (Fig. 11a), the flow stress increased when the soaking temperature increased from 520 to 550 °C but was independent of the soaking time. These trends are in line with the electrical-conductivity results in Fig. 7a and indicate that the solute content in the aluminum matrix controlled the flow stress. Similarly, the flow stress increased when the temperature increased to 580 °C for a short soaking time. However, with increasing time, the flow stress decreased dramatically from 30 MPa (2 h) to 28 MPa (6 h) and 27.7 MPa (16 h). A further increase

in temperature to 610 °C caused the flow stress to decrease even further. These results are not in line with the expected trends from the electrical-conductivity measurements for these high temperatures (Fig. 7a).

The 0.1Mn alloy (Fig. 11b) exhibited overall higher flow stresses than the base alloy for all homogenization conditions. The treatment at 520 °C resulted in the lowest flow stress. This result is consistent with the lowest solid solution level at this temperature (Fig. 7b). The flow stress increased gradually with increasing homogenization temperature from 520 to 610 °C. This is again attributed to the increase in solid solution content at higher temperatures. In addition, the flow stress decreased slightly with increasing soaking time for all temperatures, thereby matching the decrease in the Mn solute level (Fig. 7b).

Fig. 12 compares the flow stresses for the four tested Mn contents (the base, 0.03Mn, 0.06Mn, and 0.1Mn alloys) for a fixed soaking time of 6 h. The 0.1Mn alloy exhibited the highest flow stress among the four alloys. Overall, the flow stress increased with the Mn content. However, the range of the value changes was within 1 MPa. Although this effect appears quite small, it represents a flow-stress range of approximately 3%. It is known in the industrial practice that even a difference of 1% can affect the commercial extrusion productivity. Similarly to the trends observed for the base alloy in Fig. 11a, the alloys with low Mn contents (<=0.03Mn) exhibited a large decrease in the flow stress at high temperatures, namely the base alloy at >580 °C and the 0.03Mn alloy at 610 °C.

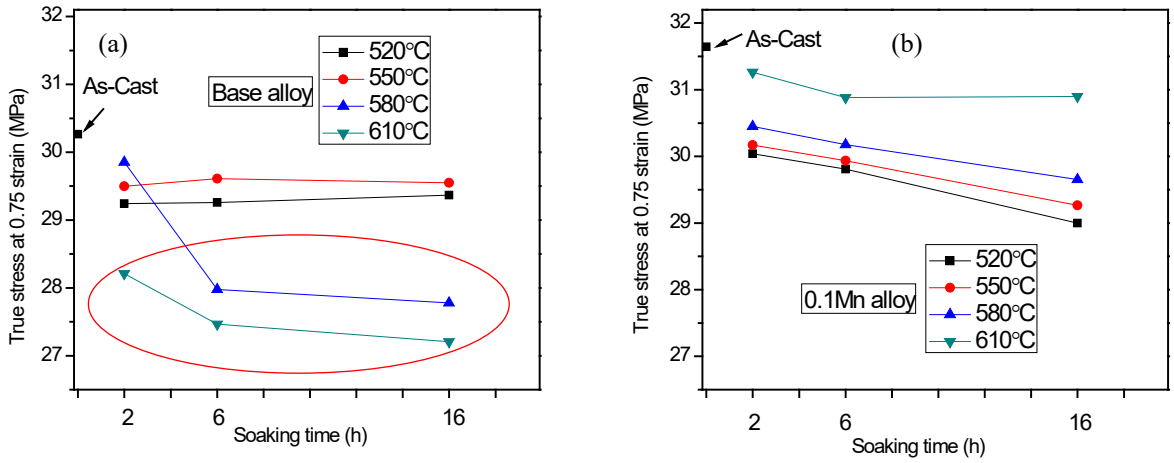

Fig. 11 Effect of homogenization conditions on the flow stress at strain of 0.75: (a) the base alloy and (b) 0.1Mn alloy

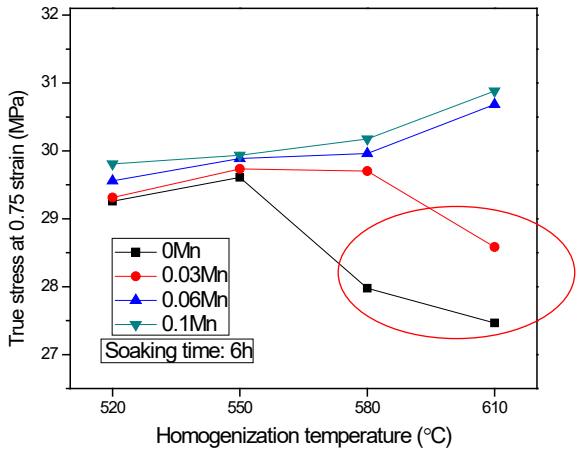

Fig. 12 Flow stress at a strain of 0.75 for different Mn contents

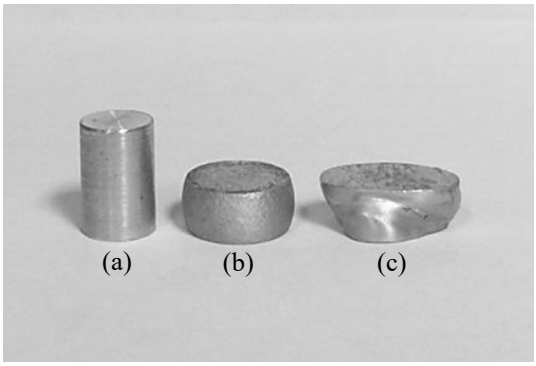

Fig. 13 Shape and appearance of compression samples: (a) cylindrical before deformation; (b) "drum" shape after deformation; (c) irregular" shape after deformation

It was observed that the deformed samples of these alloys under such treatment conditions possessed irregular shapes. Fig. 13 shows the shape and appearance of the compression samples before and after the deformation. Regarding the "normal" condition, the cylindrical samples were compressed into a "drum" shape, indicating a uniform deformation along the entire sample. However, the homogenized alloys with low Mn contents exhibiting the unusual decrease in the flow stress described above, exhibited an "irregular" shape. The homogenization conditions and related sample shape after the deformation of the base alloy are listed in Table 2. At low homogenization temperatures (520 and 550 °C), the deformed samples exhibited the drum shape. However, above 580 °C and for a soaking time of more than 6 h, the deformed samples became irregular.

For 610 °C, all deformed samples had an irregular shape. Regarding the 0.03Mn alloy, the samples homogenized at 610 °C for longer than 6 h also exhibited an irregular shape (non-uniform deformation). For Mn levels >0.06 wt.%, all deformed samples exhibited a drum shape.

Table 2 Effect of homogenization conditions on deformed sample shape – the base alloy

	2 h	6 h	16 h
520 °C	drum	drum	drum
550 °C	drum	drum	drum
580 °C	drum	irregular	irregular
610 °C	irregular	irregular	irregular

The examination of the microstructure revealed that the irregular deformed sample was related to the abnormal grain growth during the high-temperature homogenization. Fig. 14a shows the microstructure of the base alloy after the homogenization at 580 °C/2 h. Its deformation is normal and it consists of equiaxed grains with a mean size of approximately 69 μm, which is typical for as-cast 6xxx DC billets. Under applied compressive stress, the deformation can distribute in many grains with different orientations, resulting in an overall uniform deformation. Fig. 14b shows the microstructures of the base alloy homogenized at 610 °C/2 h, which exhibited an irregular shape after the deformation. Evidently, only very few giant grains remained in the entire sample section owing to the abnormal grain growth during the homogenization. The size of giant grains reached up to several millimeters. Under applied compressive stress, with this grain size, the deformation can only be directed to few grains with a limited number of slip directions. This leads to an uneven deformation in the macro scale and a decrease in the flow stress. Commercially, this condition is referred to as “giant grain” and shall be avoided because of its deleterious effect of the non-uniform deformation on the metal flow.

In addition, the grain sizes of four experiment alloys in as-cast and as-homogenized conditions were measured. The average grain sizes of the base alloy were 69 μm and 63-67 μm in the 0.03-0.1Mn alloys in the as-cast condition. After homogenization, the grain sizes remained nearly unchanged, except a few special cases mentioned above for the abnormal grain growth. Therefore, the influence of the grain sizes between different alloys on the electrical conductivity and high temperature flow stress, where no abnormal grain growth occurred, could be neglected. McQueen et al. (Ref. 22) indicated that a

change of the grain size had a relatively small effect on the flow stress during hot deformation, because the grain boundary sliding became pronounced above 300 °C in aluminum alloys and the effectiveness of grain boundary strengthening was remarkably reduced.

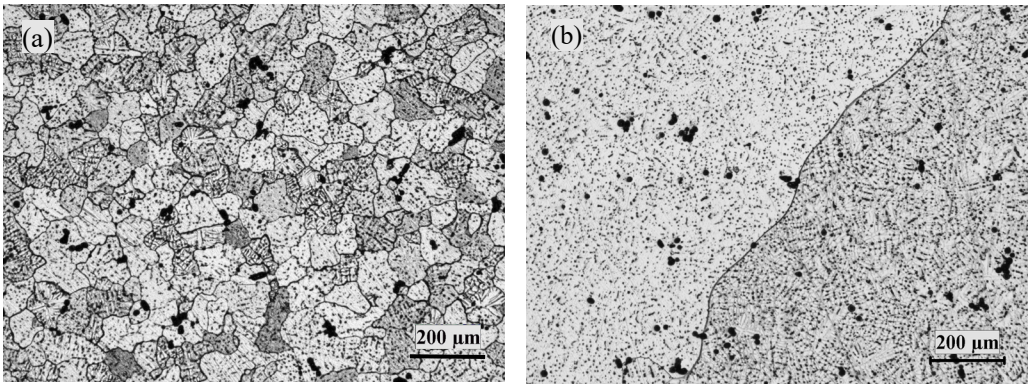

Fig. 14 Optical grain structures of the base alloy after homogenization (a) 580°C/2h, (b) 610°C/2h

3.5 Discussion

Homogenization is applied to 6xxx alloys to improve their extrusion performance in terms of extrusion pressure, speed, surface finish, and mechanical properties. In practice, these factors are interrelated. One of the key material parameters controlling the extrudability is the flow stress at the extrusion temperature. For dilute 6xxx alloys such as AA6060, which are often extruded into thin-walled profiles at high speeds, small flow stress differences of the order of 1% can have a measurable effect on the extrusion performance. In the present study, all homogenization treatments decreased the flow stress compared to the as cast condition (Fig. 11). One of the goals of the study was to optimize the homogenization time and temperature. In general, it was found that:

- The flow stress generally increased with higher homogenization temperatures for Mn contents of up to 0.10 wt.% (Fig. 11).
- The flow stress moderately increased with increasing Mn level in the alloy (Fig. 12) for a given homogenization condition.

During a hot deformation, several factors can contribute to the high-temperature flow stress. In the investigated alloys, three main microstructural features existed in the microstructures under as-cast and homogenized conditions (i.e., Fe-bearing intermetallic

particles, α-Al(FeMn)Si dispersoids, and solid solution level), which influence the hot workability of the alloy.

Fe-bearing intermetallic particles can effectively pin dislocations, which in turn changes the flow stress during a hot deformation if their particle sizes are small (<0. 1 μm) and distributed uniformly in the matrix (Ref. 22). In the present study, the Fe-bearing intermetallic particles were mainly distributed in the interdendritic region, and the interparticle spacing was very large (in the range of tens of μm (Figs. 2 and 3)). In addition, their sizes were large and ranged from one to tens of μm. Therefore, the effect of the intermetallic particles on the high-temperature flow stress is probably insignificant. However, α-Al(FeMn)Si dispersoids could possibly have a strengthening mechanism during the high-temperature deformation. Li et al. (Ref. 25) reported that a large number of dispersoids with small sizes (45–50 nm) significantly strengthened AA3004 at high temperatures. In this study, α-Al(FeMn)Si dispersoids were observed in the Mn-containing alloy (0.1Mn) after a homogenization at 520–580 °C (Fig. 6). However, owing to the low Mn level, the number density was relatively low and the dispersoid size was relatively large (of the order of 0.5 μm (Figs. 3 and 6)). It is unlikely that such a distribution could remarkably influence the dislocation motion at high temperatures. For example, the number density of dispersoids in the 0.1Mn alloy homogenized at 520 °C increased significantly with the soaking time (Fig. 6). However, the flow stress did not increase correspondingly but exhibited a decrease (Fig. 11b).

The similarity in the trends between the electrical conductivity and flow stress in Figs. 7 and 11 suggests that the flow stress is closely related to the solid solution levels. It was reported that solute elements can have a significant influence on the high-temperature flow stress by interacting with the mobile dislocations and retarding softening processes (Ref. 22, 26). Regarding the base alloy, with increasing homogenization temperature from 520 to 580 °C, the fragmentation of the Fe-bearing intermetallic, dissolution of primary Mg_2Si, and solubility of the alloying elements including Fe increased with temperature, resulting in a higher level of solute atoms in the aluminum matrix and lower electrical conductivity (Fig. 7a). Correspondingly, the flow stress increased with increasing homogenization temperature (Fig. 11a). This tendency was interrupted for the homogenization at 580 and 610 °C, in which the flow stress exhibited a sudden decrease owing to the abnormal grain growth (Table 2 and Fig. 14). However, regarding the 0.1Mn alloy (where no abnormal grain growth occurred), the solid solution level and flow stress followed the same trend for the tested homogenization conditions. Increasing the homogenization temperature from 520 to

610 °C significantly increased the solid solution level in the matrix (Fig. 7b). The flow stress exhibited a corresponding increase (Fig. 11b). In addition, the solid solution level decreased with extended soaking time for all homogenization temperatures, indicating a reduced Mn solute level in the matrix. In line with this trend, the flow stress at all homogenization temperatures also decreased slightly with increasing soaking time (Fig. 11b). The decrease in the Mn solid solution level in the matrix with extended treatment time matches the increase in the Mn/Fe ratio in the constituent particles. The same trend was reported for AA6082 (Ref. 24). Owing to these changes in the solute level and ignoring the effects of the growth of giant grains, the results of the current study suggest that the flow stress of a typical AA6060 alloy containing up to 0.10 wt.% Mn can be changed by 6% via variations in the homogenization conditions.

The incremental Mn addition from 0 to 0.1% moderately increased the flow stress at all four homogenization temperatures by approximately 1 MPa (Fig. 11c). This represents an increase in the flow stress of 3%, which is still significant in terms of commercial extrusion. Hence, micro-alloying additions of Mn can negatively impact the flow stress of an alloy. However, in commercial alloys, the micro-alloying effect of Mn is typically employed to contribute to the hot workability by facilitating the β–α intermetallic transformation. Additionally, as presented in this paper, a small Mn addition (>0.06%) effectively suppresses undesirable grain growth and enables high-temperature homogenization (above 550 °C). The precise role of the small Mn addition in preventing grain growth was not completely investigated in this work. It is probably due to the increased constituent volume fraction and number density, which result in an increase in grain boundary pinning.

The experimental results demonstrate that the homogenization treatment can reduce the flow stress and improve the hot workability. Obtaining a minimal flow stress is desirable, which directly control the extrusion speed. However, other features such as the fragmentation and transformation of Fe constituents and the removal of micro-segregations also need to be realized. Consequently, the selection of the homogenization conditions is often a trade-off. Regarding the investigated AA6060 alloys, the homogenization at a low temperature (520 °C) can reduce the flow stress owing to a low solid solution level. High-temperature homogenization (>550 °C) raises the flow stress by increasing the solid solution level. Nevertheless, it can effectively promote the fragmentation of intermetallics. Regarding the base alloy (free of Mn), the optimal homogenization treatment could be at 550 °C for 6 h, in which the flow stress is still relatively low and the Fe-bearing intermetallics become partially fragmented,

whereas the growth of giant grains is suppressed. Regarding the alloy with 0.1 wt.% Mn, a homogenization at 550–580 °C for 6 h could be the best trade-off choice to balance the flow stress and achieve the desired microstructure. Under such conditions, β-AlFeSi particles completely transform into α-AlFeSi, and the fragmentation level of the intermetallics is considerably high (Fig. 3).

4 Conclusions

(1) The β-AlFeSi intermetallic was the dominant phase in the as-cast microstructure of AA6060 alloys containing up to 0.10 wt.% Mn. During the homogenization, intermetallic fragmentation occurred, and plate-like β-AlFeSi transformed into rod-like α-AlFeSi. The micro-alloying with Mn promoted the transformation of β-AlFeSi into α-AlFeSi at lower temperatures.

(2) α-Al(FeMn)Si dispersoids were precipitated during the homogenization of the 0.1 wt.% Mn variant. The highest number density was observed at 520 °C, and coarsening and dissolution occurred above 550 °C. Owing to their low number density and relatively large size, the effect of dispersoids on the flow stress was determined to be negligible.

(3) The flow stress behavior of homogenized AA6060 alloys was mainly determined by the solid solution level. The increase in the homogenization temperature resulted in higher flow stresses owing to the increase in solute levels in the aluminum matrix.

(4) The incremental Mn addition from 0 to 0.1% moderately increased the flow stress by up to 3%. In Mn-containing alloys, the flow stress decreased with increasing soaking time owing to the long-range diffusion of Mn to the constituent particles, which exhibited a corresponding increase in the Mn/Fe ratio.

(5) The abnormal grain growth occurred in alloys with low Mn contents (<0.03Mn) during the high-temperature homogenization (580–610 °C), which resulted in a reduced flow stress and non-uniform deformation. Higher additions of Mn (>0.06%) effectively prevented this effect.

Acknowledgement

The authors would like to acknowledge the financial support from the Natural Sciences and Engineering Research Council of Canada (NSERC) and Rio Tinto Aluminum, through the NSERC Industry Research Chair in Metallurgy of Aluminum Transformation at the University of Quebec at Chicoutimi.

References

1. J. Li, A. Wimmer, G. Dehm, and P. Schumacher, Intermetallic Phase Selection During Homogenization for AA6082 Alloy, *Philosophical Magazine*, 2014, **94(8)**, p 830-846
2. S. Kumar, K.A.Q. O'Reilly, Influence of Al Grain Structure on Fe Bearing Intermetallics During DC Casting of an Al-Mg-Si Alloy, *Materials Characterization*, 2016, **120**, p 311-322
3. S. Samaras, G. Haidemenopoulos, Modelling of Microsegregation and Homogenization of 6061 Extrudable Al-alloy, *Journal of Materials Processing Technology*, 2007, 194. p 63–73
4. A. Dons, The Alstruc Homogenization Model for Industrial Aluminum Alloys, *J. Light Met.*, 2001, **1**, p 133–149
5. C. Niels, W. Kuijpers, F. Vermolen, K. Vuik, and S. Zwaag, A Model of the β-AlFeSi to α-Al(FeMn)Si Transformation in Al-Mg-Si Alloys, *Materials Transactions*, 2003, **44(7)**, p 1448-1456
6. N. Bayat, T. Carlberg, and M. Cieslar, In-situ Study of Phase Transformations During Homogenization of 6005 and 6082 Al Alloys, *Journal of Alloys and Compounds*, 2017, **725**, p 504-509
7. R. Hu, T. Ogura, H. Tezuka, T. Sato and Q. Liu, Dispersoid Formation and Recrystallization Behavior in an Al-Mg-Si-Mn Alloy, *J. Mater. Sci. Technol.*, 2010, **26(3)**, p 237-243
8. L. Lodgaard, N. Ryum, Precipitation of Dispersoids Containing Mn and/or Cr in Al–Mg–Si alloys, *Materials Science & Engineering A*, 2000, **283**, p 144-152
9. O. Reiso, Extrusion of AlMgSi Alloys, *The 9th International Conference on Aluminium Alloys*, 2004, p 32-46
10. Y. Totik, M. Gavgali, The Effect of Homogenization Treatment on the Hot Workability Between the Surface and the Center of AA 2014 Ingots, *Materials Characterization*,2003, **49**, p 261–268
11. Y. Han, K. Ma, L. Li, and W. Chen, H. Nagaumi, Study on Microstructure and Mechanical Properties of Al–Mg–Si–Cu Alloy With High Manganese Content, *Materials and Design*, 2012, **39**, p 418–424
12. A. Muggerud, E. Mortsell, Y. Li, R. Holmestad, Dispersoid Strengthening in AA3xxx Alloys with Varying Mn and Si Content During Annealing at Low Temperatures, *Materials Science & Engineering A*, 2013, **567**, p 21-28
13. Z. Li, Z. Zhang, X.-G. Chen, Effect of Magnesium on Dispersoid Strengthening of Al−Mn−Mg−Si (3xxx) Alloys, *Trans. Nonferrous Met. Soc. China*, 2016, **26**, p 2793-2799
14. N. Kuijpers, F. Vermolenb, C. Vuikb, P. Koenisc, The Dependence of the β-AlFeSi to α-Al(FeMn)Si Transformation Kinetics in Al–Mg–Si Alloys on the Alloying Elements, *Materials Science & Engineering A*, 2005, **394**, p 9-19

15. M. Shakiba, N. Parson, X.-G.Chen, Hot Deformation Behavior and Rate-controlling Mechanism in Dilute Al–Fe–Si Alloys with Minor Additions of Mn and Cu, *Materials Science & Engineering A*, 2015, **636**, p 572-581
16. P. Yu. Bryantsev, Quantitative Estimation of the Transformation of Ferrous Phases during Homogenizing Annealing of Alloys of the 6XXX Series, *Russian Journal of Non-Ferrous Metals,* 2007, **48, 6**, p 433–437
17. G. N. Haidemenopoulos, H. Kamoutsi, A. D. Zervaki, Simulation of the Transformation of Iron Intermetallics during Homogenization of 6xxx Series Extrudable Aluminum Alloys, *Journal of Materials Processing Technology*, 2012, **212**, p 2255–2260
18. C. L. Liu, H. Azizi-alizamini, N. C. Parson, W. J. Poole, Q. Du, Microstructure Evolution during Homogenization of Al−Mg−Si−Mn−Fe Alloys: Modelling and Experimental Results, *Trans. Nonferrous Met. Soc. China,* 2017, **27**, p 747−753
19. N. Kuijpers, Kinetics of the β-AlFeSi to α-Al(FeMn)Si transformation in Al-Mg-Si Alloys, PhD thesis, Delft University of Technology, 2004, p 8-10, 41-48, 49-58, 105–125 .
20. Y. Wu, J. Xiong, R. Lai, X. Zhang, Z. Guo, The Microstructure Evolution of an Al–Mg–Si–Mn–Cu–Ce Alloy During Homogenization, *Journal of Alloys and Compounds*, 2009, **475**, p 332–338
21. M. Shakiba, N. Parson, X.-G. Chen, Effect of Homogenization Treatment and Silicon Content on the Microstructure and Hot Workability of Dilute Al–Fe–Si Alloys, *Materials Science & Engineering A*, 2014, **619**, p 180–189
22. H. McQueen, S. Spigarelli, M. Kassner, E. Evagelista, Hot Deformation and Processing of Aluminum Alloys, *CRC Press, Florida*, 2011, p 14-16,87-233.
23. J. Zhang, F. Pan, R. Zuo, C. Bai, The Low Temperature Precipitation in Commercial-purity Aluminium Sheets for Foils, *Journal of Materials Processing Technology*, 2008, **206(1-3)**, p 382-387
24. C. Liu, Q. Du, N. Parson, W. Poole, The Interaction Between Mn and Fe on the Precipitation of Mn/Fe Dispersoids in Al-Mg-Si-Mn-Fe Alloys. *Scripta Materialia*, 2018, **152**, p 59-63
25. Z. Li, Z. Zhang, X.-G. Chen, Microstructure, Elevated-temperature Mechanical Properties and Creep Resistance of Dispersoid-strengthened Al-Mn-Mg 3xxx Alloys with Varying Mg and Si Contents, *Materials Science & Engineering A*, 2017,**708**, p 383-394
26. Q. Zhao, M. Slagsvold and B. Holmedal, Comparison of the Influence of Si and Fe in 99.999% Purity Aluminum and in Commercial-purity Aluminum, *Scripta Materialia*, 2017, **67**, p 217-220